Molecular Transformations in the Solid State. Crystallographic Resolution of the Spin Isomers of Tris(2-picolylamine)iron(II) Dichloride and the Structural Relationship between the Methanol and Ethanol Solvates

Bradley A. Katz and Charles E. Strouse*

Contribution from the Department of Chemistry, University of California, Los Angeles, Los Angeles, California 90024. *Received January 29, 1979*

Abstract: Multiple temperature crystallographic analysis has provided a detailed structural and thermodynamic description of the spin-state transformation in the methanol solvate of tris(2-picolylamine)iron(II) dichloride. Iron-nitrogen distances in the crystallographically resolved spin isomers are in excellent agreement with those obtained in the high- and low-temperature limits. Thermodynamic parameters obtained crystallographically agree well with those obtained spectroscopically. A two-dimensional hydrogen-bonding network links all amine hydrogen atoms of the complexes, the noncoordinating chloride ions, and the methanol molecule. Low-temperature structural analysis of the ethanol solvate of this salt reveals the same hydrogen-bonding network but a different space group. Crystal data, $Fe(2\text{-pic})_3Cl_2 \cdot MeOH$, 115 K: space group *Pbna*, $Z = 8$, $a = 11.359$ (2) Å, $b = 18.582$ (3) Å, $c = 21.873$ (4) Å, $V = 4617$ (1) Å^3, $R = 0.037$, $R_w = 0.046$ for 3107 reflections. $Fe(2\text{-pic})_3Cl_2 \cdot EtOH$, 115 K: space group $P2_1/a$ (c unique), $Z = 4$, $a = 11.389$ (5) Å, $b = 10.768$ (5) Å, $c = 21.654$ (8) Å, $\gamma = 117.18$ (3)°, $V = 2362$ (2) Å^3, $R = 0.051$, $R_w = 0.061$ for 3627 reflections.

Introduction

Many chemically and biologically significant transformations of Fe(II) or Fe(III) complexes are accompanied by a change in metal ion spin state. Since such a spin-state change drastically alters the strength of donor–metal ion interactions and hence the chemical properties of the complex, materials that exhibit some variety of "spin equilibrium" behavior, i.e., exist as an equilibrium mixture of spin isomers, have been extensively investigated.[1-6]

Magnetic, spectroscopic, kinetic, and structural techniques have been applied to the characterization of spin-state transformations both in the solid state and in solution. One solid-state approach has involved the crystallographic characterization at room temperature of a series of complexes of similar structure but variable spin state, depending on the ligand system or noncoordinating anion. Thus Sinn et al.[7] determined the structures at room temperature of the low-spin $[Fe(sal)_2trien]Cl \cdot 2H_2O$ and $[Fe(sal)_2trien]NO_3 \cdot H_2O$ and the high-spin $[Fe(acacCl)_2trien]PF_6$ and $[Fe(acac)_2trien]PF_6$ complexes, and observed a change of 0.12 Å in the average metal–ligand bond length between the high- and low-spin states.

In a few cases X-ray diffraction investigations of a single material at both high and low temperatures have provided a detailed structural description of the spin isomers. König and Watson[8] determined the structure of $Fe(2,2'\text{-bpy})_2(NCS)_2$ (polymorph II) at temperatures above and below an abrupt spin-state transition. In this complex the Fe–N bond lengths were observed to change from 2.02 Å in the $^1A_1$ state to 2.14 Å in the $^5T_2$ state. X-ray diffraction measurements reported for a complex of Fe(II) with the hexadentate ligand (4-(6-R)-2,2-bipyridyl)-3-aza-3-butenylamine[9] showed the expected decrease of about 0.12 Å in the average of the six Fe–N bond distances in the transformation from a completely high-spin state at 300 K to a mixture of high- and low-spin states at 205 K. Leipoldt and Coppens[10] have determined the structure of a trisdithiocarbamate complex of Fe(III) at 79 K, where the complex is predominantly low spin, and at room temperature where the complex contains approximately equal amounts of high-spin and low-spin iron. In all the above investigations, at temperatures where two or more isomers were present in significant amounts, only an "average" structure was reported (i.e., the spin isomers were not crystallographically resolved). While structural investigations of this type are extremely valuable, it is clear that much more detailed information would be available if the crystallographic disorder implicit in these materials could be resolved, and the structural determination carried out over a range of temperatures.

Recent investigations[11,12] in this laboratory have demonstrated the power of multiple-temperature X-ray structural analysis as a probe of the structural, thermodynamic, and mechanistic aspects of several chemically important classes of molecular transformations. Among the various types of molecular transformations currently under investigation, the spin-state transformations of transition-metal complexes perhaps best illustrate the utility and comprehensive nature of the information available from these techniques.

Although many transition-metal complexes exhibit spin-equilibrium behavior, the choice of subject compounds for the current investigation was dictated by a number of specific goals. An initial goal was the demonstration that crystallographic resolution of spin isomers is indeed feasible.[12] To this end a series of complexes was chosen with relatively rigid ligands so that the resolution would involve the location of a few ligand molecules rather than many individual atoms. In addition, the initial selection was limited to those materials which exhibit a 50:50 mixture of high- and low-spin species at a temperature near the lowest accessible with available diffraction equipment. This constraint minimizes the deleterious effects of thermal motion. Magnetic properties of various solvates of tris(2-picolylamine)iron(II) chlorides reported by Renovitch and Baker[13] and by Sorai et al.[14] suggested that several of these materials would satisfy the above criteria. The crystallographic investigation reported here is based on structural determinations of the methanol solvate of tris(2-picolylamine)iron(II) dichloride at five temperatures and of the ethanol solvate at low temperature.[33]

Experimental Section

Sample Preparation. $Fe(2\text{-pic})_3Cl_2 \cdot MeOH$. $Fe(2\text{-pic})_3Cl_2 \cdot MeOH$ was prepared by slow evaporation of a methanol solution of $Fe(2\text{-pic})_3Cl_2 \cdot 2H_2O$ under a nitrogen atmosphere. The resulting crystals

0002-7863/79/1501-6214$01.00/0

Table I. Summary of Experimental Parameters[a]

				$Fe(2\text{-pic})_3Cl_2\cdot MeOH$					
temp,[c] K	a	b	c	V	R	R_w	no. obsd[b] refl	EOF[b]	low-spin fraction[b]
115	11.359 (2)	18.582 (3)	21.873 (4)	4617 (1)	0.037	0.046	3107	1.45	0.964 (9)
148	11.396 (3)	18.680 (4)	22.034 (6)	4691 (2)	0.041	0.051	3044	1.53	0.609 (19)
171	11.401 (2)	18.701 (5)	22.115 (5)	4715 (2)	0.041	0.050	2989	1.46	0.338 (19)
199	11.457 (3)	18.768 (6)	22.298 (4)	4795 (2)	0.037	0.047	1757	1.52	0.183 (20)
227	11.445 (3)	18.752 (6)	22.282 (5)	4782 (2)	0.041	0.054	1920	1.68	0.164 (19)

			$Fe(2\text{-pic})_3Cl_2\cdot EtOH$						
temp, K	a	b	c	γ	V	R	R_w	no. obsd[b] refl	EOF[b]
115	11.389 (5)	10.768 (5)	21.654 (8)	117.18 (3)	2362 (2)	0.051	0.061	3627	1.69

[a] In this and all subsequent tables, the estimated standard deviations of the last significant figures are given in parentheses. Expressions for R and R_w are given in footnote 19. [b] Observed reflections are those with $I > 3\sigma(I)$; EOF is the standard deviation in an observation of unit weight. The low-spin fractions are the refined occupancy factors of the low-spin rigid groups with the sum of the low-spin and high-spin occupancy factors constrained to unity. [c] The methanol solvate was cooled from room temperature to 115 K and the experimental parameters at 115 K were then determined. The parameters at 148, 171, and 227 K were obtained as the crystal was warmed from 115 K, whereas those at 227 K were obtained when the crystal was cooled back down from room temperature (see text).

appeared straw colored under the microscope. The crystals decomposed to a red, amorphous material upon prolonged exposure to air at room temperature. Crystals were attached to glass fibers and transferred quickly into the nitrogen stream of a locally constructed variable-temperature apparatus[15] mounted on a Syntex $P\bar{1}$ diffractometer. Upon cooling, the crystals turned bright red at about 150 K. The straw color could be restored by heating to room temperature. As the crystals were cooled slowly from room temperature, an intense X-ray reflection was scanned after each small decrement in temperature. All crystals fractured, however, near the transition temperature as evidenced by splitting of the Bragg peak. The crystal used in the structural analysis was obtained by chipping off a portion of a fractured crystal with a glass fiber while the crystal was mounted on the diffractometer. The resulting irregularly shaped single crystal had the approximate dimensions 0.45 × 0.20 × 0.20 mm with the long axis approximately collinear with the φ axis of the goniometer.

Data Collection. X-ray diffraction data were collected at five different temperatures starting at 115 K with monochromatized Mo Kα radiation (λ 0.710 70 Å). Temperature measurements were made after the data collection with a thermocouple mounted in the cold stream and with the heater voltage reset to the values used for the data collection. The fluctuation in temperature at 115 K was less than 1 K; at higher temperatures the fluctuation was about 2 K. This temperature instability arose from the change in nitrogen level in the reservoir of the low-temperature apparatus. The temperature fluctuation was approximately sinusoidal in time with a period of about 1 h. All temperature measurements were averaged over two or more periods. All temperature settings were reproducible to within 1 K.

Lattice parameters and their estimated standard deviations were obtained from a least-squares fit of 15 automatically centered reflections with $28° < 2\theta < 35°$. Comparison of the volume of the unit cell with that of $Fe(2\text{-pic})_3Cl_2\cdot 2H_2O$[16] implied 8 molecules per unit cell. The systematic absences $0kl$, $k = 2n + 1$, $h0l$, $h + l = 2n + 1$, and $hk0$, $h = 2n + 1$, led to the space-group assignment *Pbna*, a nonstandard setting of *Pban* (D_{2h}^4, no. 50).[17] At 115, 148, and 171 K, octants of data were collected in the θ–2θ scan mode to $2\theta_{max} = 50°$. At 227 K an octant was collected to $2\theta_{max} = 35°$ along with part of the shell from 35 to 55° with $h \leq 4$, at which point the crystal was inadvertently warmed to room temperature. Upon subsequent cooling to 227 K, a hysteresis in the spin transition was observed; the lattice parameters remained larger than they had been when this temperature was approached from the lower limit. Further cooling to 199 K yielded lattice parameters still slightly greater than those at 227 K.[28] An octant of data to $2\theta_{max} = 40°$ was collected at this temperature.

Previously described data-handling procedures[18] were employed in this work. For all data sets the reflections were scanned at 3.0 deg/min from 1.0° below Kα_1 to 1.0° above Kα_2. No absorption correction was made. All reflections for which the intensity was greater than three times the estimated standard deviation were used in the least-squares refinement of the structure. In Table I is a summary of experimental parameters.

$Fe(2\text{-pic})_3Cl_2\cdot EtOH$. Evaporation under nitrogen of an ethanolic solution of $Fe(2\text{-pic})_3Cl_2\cdot 2H_2O$ afforded yellow, monoclinic crystals of $Fe(2\text{-pic})_3Cl_2\cdot EtOH$ that turned red upon cooling. Lattice parameters at 115 K are tabulated in Table I. The crystallographic a and c axes in the ethanol solvate (space group $P2_1/a$ (c unique)) are very similar in length to the corresponding axes in the methanol solvate. Moreover, the symmetry in the c direction is the same for both lattices. X-ray diffraction data for the ethanol solvate were collected at 115 K as described above for the methanol solvate.

Solution and Refinement of the Structures. The structure at 115 K was solved and refined by standard Patterson, Fourier, and least-squares techniques.[19] Scattering factors were taken from the International Tables for X-ray Crystallography.[17]

Anomalous dispersion corrections for iron and chlorine were used in all structure-factor calculations. After initial refinement to $R = 0.052$, $R_w = 0.083$, estimated positions for all nonmethanolic hydrogen atoms were calculated (C–H and N–H = 1.00 Å). These atoms were assigned isotropic thermal parameters of 3.0 Å^2 and included in subsequent structure-factor calculations.

Initial refinements with the higher temperature data sets showed increased Fe–N bond lengths and provided rough estimates of the fraction of low- and high-spin complexes at each temperature. The diffraction data were then used to refine a model containing a single iron atom surrounded by both low- and high-spin ligands. Low-spin ligands were represented by three "semirigid" groups, whose initial positional, orientational, and thermal parameters were obtained from the refinement at 115 K, where the complex is essentially all low spin. Positional, orientational, and thermal parameters for three analogous high-spin groups were derived from a refinement of the data set at 199 K, where the complex is predominantly, albeit not entirely, high spin. At 148 K, the initial x, y, and z coordinates for the high-spin rigid group origins were calculated by multiplication of the x, y, and z coordinates obtained at 199 K by the ratios a_{148K}/a_{199K}, b_{148K}/b_{199K}, and c_{148K}/c_{199K}, respectively. The initial orientational parameters at 148 K were the same as those used at 199 K. The refined orientational parameters at 148 K were used as initial orientational parameters at 171 K. The refined positional parameters at 148 K were altered as above to correspond to the unit cell at 171 K and used to begin the refinement at 171 K. Analogous procedures yielded initial group coordinates and orientational parameters for each temperature and spin state.

In the refinement at 199 K that provided the structural parameters of the high-spin rigid groups, the positional and anisotropic thermal parameters of all nonhydrogen atoms were refined, while the nonmethanolic hydrogen atomic positional and isotropic thermal parameters were fixed (C–H = 1.00 Å, N–H = 1.00 Å, $B = 2.00$ Å^2). The methanolic hydrogen positions were obtained from the refinement without groups at 115 K; their positional parameters were refined with fixed isotropic thermal parameters of 10.0 Å^2.

During the initial least-squares cycles with rigid groups, only the positional, orientational, and isotropic group thermal parameters were refined; the initial thermal parameters of all low-spin groups were set equal to 2.4 Å,^{2} which was an average of the isotropic thermal pa-

Table II. Atomic Positions and Temperature Factors for $Fe(2\text{-pic})_3Cl_2 \cdot MeOH$ (115 K)[a]

atom	x	y	z	$\beta_{11} \times 10^5$	$\beta_{22} \times 10^5$	$\beta_{33} \times 10^5$	$\beta_{12} \times 10^5$	$\beta_{13} \times 10^5$	$\beta_{23} \times 10^5$
Cl1	0.3731 (7)	0.0673 (4)	0.4300 (4)	248 (6)	162 (3)	92 (2)	48 (3)	17 (3)	27 (2)
Cl2	0.4723 (7)	0.3640 (4)	0.2272 (4)	381 (7)	134 (2)	98 (2)	−7 (3)	32 (3)	−9 (2)
Fe	0.2060 (4)	−0.0100 (2)	0.1345 (2)	215 (4)	97 (1)	59 (1)	7 (2)	0 (2)	−2 (1)
N1	0.3611 (23)	0.0271 (13)	0.1050 (12)	257 (21)	98 (8)	59 (6)	8 (10)	0 (9)	0 (5)
N2	0.1519 (23)	0.0301 (14)	0.0531 (12)	242 (21)	111 (8)	68 (6)	10 (11)	5 (9)	−3 (5)
N3	0.0397 (23)	−0.0462 (14)	0.1485 (12)	299 (22)	121 (8)	82 (6)	10 (11)	18 (10)	11 (6)
N4	0.2669 (23)	−0.0451 (14)	0.2172 (12)	257 (22)	121 (8)	70 (6)	11 (11)	−1 (9)	4 (6)
N5	0.2269 (22)	−0.1092 (14)	0.1015 (12)	272 (22)	117 (8)	53 (5)	−5 (11)	−5 (9)	2 (5)
N6	0.1710 (23)	0.0781 (14)	0.1844 (12)	286 (22)	116 (8)	70 (6)	0 (11)	−12 (9)	5 (6)
C1	0.5731 (28)	0.0344 (18)	0.0984 (16)	270 (26)	146 (10)	97 (8)	−8 (13)	−14 (12)	−15 (7)
C2	0.5652 (29)	0.0791 (18)	0.0474 (16)	306 (27)	151 (11)	100 (8)	−62 (14)	−9 (12)	−2 (7)
C3	0.3555 (28)	0.0710 (17)	0.0551 (15)	296 (26)	96 (9)	80 (7)	−6 (13)	−6 (11)	−15 (7)
C4	0.4703 (27)	0.0106 (18)	0.1256 (14)	247 (25)	144 (10)	82 (7)	−9 (13)	−21 (11)	−7 (7)
C5	0.2332 (28)	0.0884 (18)	0.0333 (15)	241 (26)	136 (10)	94 (7)	10 (13)	−2 (11)	16 (7)
C6	0.4548 (29)	0.0979 (17)	0.0259 (15)	330 (27)	127 (10)	93 (8)	−10 (14)	15 (12)	−2 (7)
C7	0.3305 (28)	−0.1440 (18)	0.0936 (15)	341 (27)	140 (10)	57 (7)	42 (13)	6 (11)	4 (7)
C8	0.3371 (32)	−0.2172 (18)	0.0800 (16)	490 (30)	134 (10)	84 (8)	64 (15)	19 (12)	5 (7)
C9	0.2346 (34)	−0.2561 (19)	0.0748 (15)	705 (35)	102 (10)	74 (8)	1 (16)	16 (13)	3 (7)
C10	0.1281 (32)	−0.2213 (18)	0.0829 (16)	513 (31)	138 (10)	78 (7)	−73 (15)	−3 (12)	6 (7)
C11	0.1263 (29)	−0.1479 (18)	0.0959 (15)	330 (26)	148 (10)	64 (7)	−45 (14)	−12 (12)	13 (7)
C12	0.0152 (29)	−0.1056 (18)	0.1054 (16)	279 (26)	155 (11)	111 (8)	−23 (14)	−3 (12)	9 (8)
C13	0.0933 (29)	0.1314 (17)	0.1712 (15)	303 (27)	118 (10)	106 (8)	22 (13)	−26 (12)	0 (7)
C14	0.0703 (32)	0.1880 (18)	0.2107 (16)	486 (32)	126 (10)	108 (8)	56 (15)	−9 (13)	1 (7)
C15	0.1294 (34)	0.1914 (19)	0.2662 (16)	596 (34)	156 (11)	98 (8)	44 (16)	0 (14)	−16 (8)
C16	0.2069 (32)	0.1362 (19)	0.2809 (15)	487 (32)	164 (11)	79 (7)	13 (16)	−27 (13)	−12 (7)
C17	0.2241 (29)	0.0805 (17)	0.2400 (15)	301 (27)	129 (10)	82 (7)	−9 (13)	−2 (11)	1 (7)
C18	0.3033 (29)	0.0180 (18)	0.2543 (15)	329 (26)	162 (10)	65 (7)	21 (14)	−38 (11)	−15 (7)
C19	0.2996 (56)	0.2692 (31)	0.1078 (35)	1280 (66)	262 (18)	437 (22)	−252 (29)	−211 (31)	13 (16)
O	0.3514 (40)	0.3355 (23)	0.1032 (15)	1692 (48)	495 (16)	147 (8)	−550 (24)	−81 (17)	46 (9)

atom	x	y	z	B
OH	0.3531 (765)	0.3468 (488)	0.1368 (347)	10.00 (0)
C19H1	0.2492 (736)	0.2673 (508)	0.1345 (372)	10.00 (0)
C19H2	0.3537 (676)	0.2317 (434)	0.1322 (364)	10.00 (0)
C19H3	0.2304 (713)	0.2590 (451)	0.0731 (339)	10.00 (0)
C1H	0.6551 (0)	0.0189 (0)	0.1156 (0)	3.00 (0)
C4H	0.4804 (0)	−0.0209 (0)	0.1637 (0)	3.00 (0)
C2H	0.6372 (0)	0.0985 (0)	0.0263 (0)	3.00 (0)
C6H	0.4528 (0)	0.1306 (0)	−0.0129 (0)	3.00 (0)
C13H	0.0455 (0)	0.1282 (0)	0.1316 (0)	3.00 (0)
C14H	0.0110 (0)	0.2277 (0)	0.1973 (0)	3.00 (0)
C15H	0.1165 (0)	0.2355 (0)	0.2951 (0)	3.00 (0)
C16H	0.2492 (0)	0.1355 (0)	0.3230 (0)	3.00 (0)
C7H	0.4072 (0)	−0.1181 (0)	0.0995 (0)	3.00 (0)
C8H	0.4148 (0)	−0.2412 (0)	0.0739 (0)	3.00 (0)
C9H	0.2377 (0)	−0.3091 (0)	0.0642 (0)	3.00 (0)
C10H	0.0512 (0)	−0.2504 (0)	0.0782 (0)	3.00 (0)
C5H1	0.2287 (0)	0.0934 (0)	−0.0137 (0)	3.00 (0)
C5H2	0.2016 (0)	0.1364 (0)	0.0497 (0)	3.00 (0)
C12H1	−0.0501 (0)	−0.1388 (0)	0.1227 (0)	3.00 (0)
C12H2	−0.0169 (0)	−0.0865 (0)	0.0654 (0)	3.00 (0)
C18H1	0.2975 (0)	0.0056 (0)	0.3001 (0)	3.00 (0)
C18H2	0.3879 (0)	0.0300 (0)	0.2461 (0)	3.00 (0)
N4H1	0.2019 (0)	−0.0725 (0)	0.2395 (0)	3.00 (0)
N4H2	0.3346 (0)	−0.0792 (0)	0.2117 (0)	3.00 (0)
N2H1	0.1529 (0)	−0.0091 (0)	0.0210 (0)	3.00 (0)
N3H1	0.0308 (0)	−0.0638 (0)	0.1921 (0)	3.00 (0)
N2H2	0.0689 (0)	0.0485 (0)	0.0564 (0)	3.00 (0)
N3H2	−0.0186 (0)	−0.0057 (0)	0.1425 (0)	3.00 (0)

[a] The form of the anisotropic temperature factor is $\exp[-(\beta_{11}h^2 + \beta_{22}k^2 + \beta_{33}l^2 + 2\beta_{12}hk + 2\beta_{13}hl + 2\beta_{23}kl)]$.

rameters of all nonhydrogen group atoms. A value of 3.3 Å^2 was used for the high-spin rigid groups. At 148 and 171 K the isotropic temperature factors of the individual nonhydrogen group atoms were refined after convergence of the group temperature factors. The low-spin and high-spin group hydrogen temperature factors were fixed at values 10% greater than the refined low-spin and high-spin group temperature factors, respectively. At 115 K the low-spin positional parameters and the individual nonhydrogen low-spin isotropic thermal parameters were refined with all high-spin parameters fixed. In this refinement, high-spin positional parameters and individual high-spin isotropic thermal parameters derived from the refinement at 171 K were used. At 199 and 227 K the positional parameters and individual isotropic thermal parameters of the high-spin groups were refined along with the positional parameters and group temperature factors of the low-spin rigid groups.

In the rigid group refinements all group atoms associated with the same spin state were constrained to have the same occupancy, and the sum of the low-spin and high-spin occupancies was constrained to unity. "Rotational" freedom about the methylene carbon to ring carbon bond was provided by refinement of a single linear distortion parameter for each high- and low-spin group.[20]

At the three lower temperatures, the positional parameters of the

Table III. Distances of Motion of Group Atoms and Isotropic Thermal Parameters for the High- and Low-Spin States of $Fe(2\text{-pic})_3Cl_2 \cdot MeOH$ at 171 K

atom	distance, Å	low-spin B, Å^2	high-spin B, Å^2
		Group 1	
N6	0.21 (1)	2.9 (4)	2.2 (2)
C13	0.31 (1)	2.2 (3)	2.7 (2)
C14	0.37 (1)	2.4 (3)	2.8 (1)
C15	0.32 (2)	3.4 (3)	3.2 (2)
C16	0.21 (1)	3.0 (4)	3.0 (2)
C17	0.15 (1)	2.3 (5)	2.4 (2)
C18	0.21 (1)	1.7 (3)	3.0 (2)
N4	0.18 (2)	1.9 (4)	2.1 (2)
		Group 2	
N1	0.24 (1)	1.8 (2)	1.9 (1)
C4	0.25 (1)	2.3 (3)	2.0 (1)
C1	0.26 (1)	2.8 (3)	2.3 (2)
C2	0.28 (1)	2.0 (3)	2.6 (2)
C6	0.25 (1)	2.2 (3)	2.4 (2)
C3	0.22 (1)	2.4 (3)	1.9 (2)
C5	0.22 (1)	2.3 (3)	2.7 (2)
N2	0.25 (2)	1.8 (3)	2.0 (2)
		Group 3	
N5	0.14 (1)	2.9 (5)	1.8 (2)
C7	0.12 (1)	3.1 (6)	2.2 (3)
C8	0.27 (1)	3.3 (4)	2.6 (2)
C9	0.35 (2)	2.6 (3)	1.8 (1)
C10	0.35 (1)	2.6 (3)	2.6 (1)
C11	0.25 (1)	2.6 (3)	2.1 (1)
C12	0.41 (1)	2.5 (2)	2.6 (1)
N3	0.44 (2)	2.2 (2)	2.0 (1)

OH hydrogen atom were refined with the isotropic thermal parameter fixed at 10 Å^2; both positional and isotropic thermal parameters of the methyl hydrogens of methanol were refined. At the two higher temperatures the isotropic thermal parameters of all methanol hydrogens were fixed at 10 Å^2, and only their positional parameters refined. Chemically reasonable positions for all methanolic hydrogens were obtained in the refinement at 115 K,[21] but at higher temperatures the OH hydrogen atom and one of the methyl hydrogen atoms did not refine to chemically reasonable positions, presumably because of the large thermal motion of the methanol molecule.

In all refinements the chlorine, iron, oxygen, and methanol carbon atoms were assigned anisotropic thermal parameters. At 171 K, where roughly equal amounts of low- and high-spin molecules exist in equilibrium, a refinement, without constraints, of positional parameters for all low-spin and high-spin atoms with fixed isotropic temperature factors and with fixed occupancy factors was unsuccessful, leading to chemically unreasonable bond lengths. Similarly, attempts to refine the positions of two iron atoms with fixed isotropic thermal parameters were unsuccessful.

The final residual at 115 K was 0.037 ($R_w = 0.046$) and the largest peak in the final difference Fourier map was 0.6 e/Å^3 in the vicinity of C19-H3. Table II gives atomic positions and temperature factors as determined in the final least-squares cycle at 115 K. Final positions and temperature factors at other temperatures are available as supplementary data. Table III provides distances of motion of all nonhydrogen group atoms occurring with the change in spin state, at 171 K. A listing of observed structure factor amplitudes based on the parameters of the final least-squares refinements is available as supplementary data.

The structure of the ethanol solvate was solved and refined by standard Patterson, Fourier, and least-squares techniques. The spin isomers were not crystallographically resolved, although at 115 K, where the thermal motion is greatly reduced and where nearly equal amounts of low-spin and high-spin isomers are present (vide infra), such a resolution should be facile. Positional and thermal parameters determined in the last least-squares cycle at 115 K are included in the supplementary data.

Description of the Resolved Spin Isomers

The complex in the methanol solvate of tris(2-picolylamine)iron(II) dichloride has the mer geometry depicted in Figure 1. Both high-spin and low-spin ligands were resolved and refined in structure determinations at four different temperatures in the range 148–227 K. A summary of Fe–N distances and N–Fe–N angles for all determinations is provided in Table IV and a drawing of the resolved spin isomers at 171 K appears in Figure 2. Table V provides bond distances and bond angles for the 2-picolylamine ligands in the low- and high-spin state at 115 and 199 K, respectively. The degree to which the spin isomers were successfully resolved in this investigation is best demonstrated by comparison of the structural parameters obtained at 148 and 171 K, where significant amounts of both isomers are present, with those obtained at the high- and low-temperature limits. The average low-spin iron–nitrogen distances at 148 and 171 K, respectively, are 2.01 (1) and 2.02 (2) Å, compared with the distance of 2.016 (3) Å obtained for the structure at 115 K, where the material is 96% low spin. The average high-spin iron–nitrogen distances at 148 and 171 K, respectively, are 2.18 (1) and 2.19 (1) Å, compared with a value of 2.198 (6) Å obtained at 227 K, where the material is 84% high spin. The difference in the Fe–N(pyridine) bond distances observed here (2.000 (3) Å low spin vs. 2.199 (4) Å high spin) is similar to that found for Fe(II) $bpy_2(NCS)_2$[8] (2.02 Å low spin at 100 K vs. 2.14 Å at 293 K).

An average low-spin Fe–N distance of 2.016 (3) Å at 115 K agrees well with the distance of 2.007 Å found for the fac isomer of the same ion in tris(2-picolylamine)iron(II) dichloride dihydrate both at 115 K and at room temperature. Similarly, the average Fe–N distance of 2.198 (6) Å at 227 K corresponds closely to the 2.200 (7) Å distance found for the

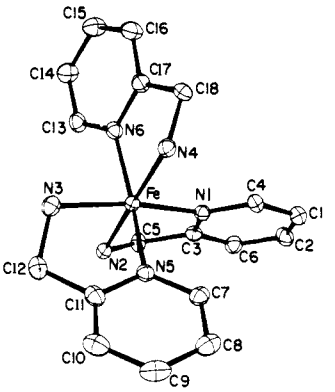

Figure 1. ORTEP drawing[19] of the $Fe(2\text{-pic})_3^{2+}$ complex of the methanol solvate at 115 K showing the labeling scheme. The observed thermal motion reflects a small high-spin component at this temperature. In this and other structural diagrams hydrogen atoms have been omitted for clarity.

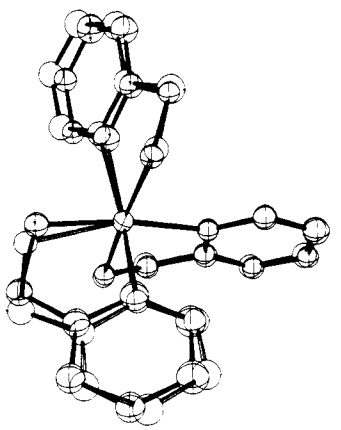

Figure 2. ORTEP diagram of the resolved spin isomers of $Fe(2\text{-pic})_3Cl_2 \cdot MeOH$ at 171 K with isotropically refined thermal parameters of group atoms.

Table IV. Iron-Nitrogen Bond Lengths and Bond Angles in Low-Spin and High-Spin $Fe(2\text{-pic})_3Cl_2 \cdot MeOH$[a]

	unresolved	low-spin					high-spin			
	115 K	115 K	148 K	171 K	199 K	227 K	148 K	171 K	199 K	227 K
					Bond Lengths (Å)					
	no groups									
amine										
Fe-N(2)[c]	2.026 (3)	2.027 (3)	1.990 (8)	1.97 (1)	2.03 (1)	2.05 (5)	2.208 (12)	2.202 (7)	2.197 (9)	2.187 (9)
Fe-N(3)	2.028 (3)	2.026 (2)	1.971 (5)	1.94 (2)	1.96 (3)	1.98 (3)	2.254 (7)	2.219 (5)	2.213 (5)	2.204 (5)
Fe-N(4)[c]	2.044 (3)	2.043 (2)	2.051 (9)	2.07 (2)	1.99 (11)	2.05 (5)	2.177 (16)	2.177 (8)	2.212 (19)	2.206 (7)
Fe-N(amine)	2.033 (3)	2.032 (2)	2.004 (7)	1.99 (2)	1.99 (6)	2.03 (5)	2.213 (12)	2.199 (7)	2.207 (11)	2.199 (7)
pyridine										
Fe-N(1)	1.999 (3)	1.999 (2)	2.027 (5)	2.07 (1)	2.14 (2)	2.15 (3)	2.153 (8)	2.183 (4)	2.212 (4)	2.211 (5)
Fe-N(5)[c]	1.993 (3)	1.993 (2)	2.006 (6)	2.04 (1)	2.11 (2)	2.14 (2)	2.142 (8)	2.161 (5)	2.180 (4)	2.176 (4)
Fe-N(6)[c]	2.007 (3)	2.008 (2)	2.017 (5)	2.05 (1)	2.13 (3)	2.13 (3)	2.170 (8)	2.187 (5)	2.205 (5)	2.205 (5)
Fe-N(pyridine)	2.000 (3)	2.000 (2)	2.017 (5)	2.05 (1)	2.13 (2)	2.14 (3)	2.155 (8)	2.180 (5)	2.199 (4)	2.197 (5)
Fe-N(av)	2.016 (3)	2.016 (2)	2.011 (6)	2.02 (2)	2.06 (4)	2.09 (4)	2.184 (10)	2.190 (6)	2.203 (8)	2.198 (6)
					Bond Angles (deg)					
N(1)-Fe-N(2)	81.8 (1)	81.74 (6)	82.1 (2)	81.2 (3)	80 (1)	77 (1)	76.1 (3)	75.9 (2)	75.5 (2)	75.7 (2)
N(3)-Fe-N(5)	81.9 (1)	82.01 (7)	82.9 (2)	82.5 (7)	80 (1)	79 (1)	76.6 (3)	76.8 (2)	76.4 (2)	76.6 (2)
N(4)-Fe-N(6)	81.1 (1)	81.08 (7)	80.3 (2)	78.6 (4)	78 (2)	77 (1)	77.0 (4)	76.5 (2)	75.2 (3)	75.6 (2)
N(1)-Fe-N(4)	95.5 (1)	95.55 (8)	94.1 (3)	94.0 (5)	93 (3)	100 (1)	96.7 (4)	95.5 (2)	95.8 (4)	94.6 (2)
N(1)-Fe-N(5)	95.5 (1)	95.49 (7)	95.1 (2)	94.3 (4)	94 (1)	96 (1)	96.9 (3)	97.1 (2)	97.6 (2)	97.3 (2)
N(1)-Fe-N(6)	93.9 (1)	93.92 (7)	93.3 (2)	95.1 (4)	98 (1)	103 (1)	96.5 (3)	95.9 (2)	95.8 (2)	95.1 (2)
N(2)-Fe-N(3)	88.4 (1)	88.42 (8)	90.3 (2)	91.3 (7)	91 (1)	91 (1)	85.9 (3)	87.0 (2)	88.1 (2)	87.8 (2)
N(2)-Fe-N(5)	93.4 (1)	93.29 (8)	94.1 (3)	95.2 (6)	95 (1)	96 (2)	96.2 (5)	97.2 (3)	98.1 (3)	97.9 (3)
N(2)-Fe-N(6)	96.8 (1)	96.82 (8)	97.8 (3)	99.7 (4)	100 (1)	102 (2)	96.9 (4)	97.1 (2)	98.1 (2)	97.5 (3)
N(3)-Fe-N(4)	94.4 (1)	94.40 (9)	93.6 (3)	93.6 (7)	98 (3)	92 (2)	102.2 (4)	102.3 (2)	101.4 (4)	102.8 (2)
N(3)-Fe-N(6)	90.2 (1)	90.22 (8)	90.2 (2)	89.8 (7)	91 (1)	86 (1)	93.9 (3)	94.2 (2)	94.4 (2)	95.3 (2)
N(4)-Fe-N(5)	89.1 (1)	89.20 (7)	88.3 (3)	87.1 (5)	88 (2)	85 (1)	91.3 (4)	90.8 (2)	90.2 (3)	90.7 (2)
N(1)-Fe-N(3)	169.7 (1)	169.71 (8)	172.0 (2)	171.6 (7)	167 (1)	166 (1)	160.1 (3)	161.1 (2)	161.7 (2)	161.5 (2)
N(2)-Fe-N(4)	176.5 (1)	176.47 (8)	175.7 (3)	174.8 (5)	171 (2)	177 (1)	170.1 (4)	168.9 (2)	168.6 (3)	167.7 (2)
N(5)-Fe-N(5)	167.0 (1)	167.08 (7)	166.3 (3)	163.4 (5)	162 (1)	156 (1)	163.1 (4)	162.6 (2)	161.1 (2)	162.3 (2)
Fe-N(pyridine)-C_u[b]	127.4 (2)	127.4 (2)	127.5 (2)	128.4 (7)	129 (2)	128 (2)	125 (2)	125 (2)	125.3 (5)	125.4 (5)
Fe-N(pyridine)-C_s[b]	115.1 (2)	115.1 (2)	115.0 (2)	114.4 (6)	114 (2)	113 (3)	116 (2)	116 (2)	116.0 (4)	116.0 (5)
Fe-N(amine)-C[b]	109.2 (2)	109.2 (1)	109.3 (4)	111 (1)	114 (2)	113 (2)	109 (2)	109.8 (11)	110.0 (11)	110.6 (11)

[a] Uncertainties in bond length averages are the averages of the individual esd's. [b] Averages of the angles for the three ligands where u denotes unsubstituted ring carbon and s denotes substituted ring carbon. [c] Trans.

Table V. Bonding Distances (Å) and Angles (deg) within the 2-Picolylamine Ligands of $Fe(2\text{-pic})_3Cl_2 \cdot MeOH$

distances	115 K (low spin)	119 K (high spin)	angles	115 K (low spin)	199 K (high spin)
N(2)-C(5)	1.487 (4)	1.475 (7)	N(2)-C(5)-C(3)	108.9 (3)	110.3 (5)
N(3)-C(12)	1.477 (4)	1.473 (7)	N(3)-C(12)-C(11)	108.7 (3)	111.7 (5)
N(4)-C(18)	1.484 (4)	1.492 (7)	N(4)-C(18)-C(17)	109.3 (3)	111.3 (5)
N(1)-C(4)	1.356 (4)	1.354 (7)	C(5)-C(3)-C(6)	121.8 (3)	120.7 (5)
N(1)-C(3)	1.364 (4)	1.332 (7)	C(12)-C(11)-C(10)	123.6 (3)	122.5 (5)
N(5)-C(7)	1.354 (4)	1.342 (7)	C(18)-C(17)-C(16)	122.0 (3)	121.3 (5)
N(5)-C(11)	1.356 (4)	1.352 (7)	C(3)-C(6)-C(2)	119.2 (3)	118.4 (5)
N(6)-C(13)	1.357 (4)	1.357 (7)	C(11)-C(10)-C(9)	119.8 (3)	120.2 (5)
N(6)-C(17)	1.359 (4)	1.350 (7)	C(17)-C(16)-C(15)	119.5 (3)	119.2 (5)
C(3)-C(5)	1.504 (4)	1.518 (7)	C(6)-C(2)-C(1)	118.8 (3)	119.8 (5)
C(11)-C(12)	1.502 (5)	1.486 (9)	C(10)-C(9)-C(8)	119.0 (3)	119.3 (5)
C(17)-C(18)	1.501 (5)	1.481 (9)	C(16)-C(15)-C(14)	118.3 (3)	119.7 (5)
C(3)-C(6)	1.390 (4)	1.381 (8)	C(2)-C(1)-C(4)	118.7 (3)	117.4 (5)
C(6)-C(2)	1.384 (5)	1.378 (9)	C(9)-C(8)-C(7)	119.0 (3)	118.2 (5)
C(2)-C(1)	1.393 (5)	1.401 (9)	C(15)-C(14)-C(13)	119.3 (3)	118.3 (5)
C(1)-C(4)	1.384 (5)	1.373 (9)			
C(11)-C(10)	1.394 (5)	1.385 (9)	C(1)-C(4)-N(1)	123.8 (3)	123.4 (5)
C(10)-C(9)	1.383 (5)	1.372 (9)	C(8)-C(7)-N(5)	122.7 (3)	123.2 (5)
C(9)-C(8)	1.376 (5)	1.378 (9)	C(14)-C(13)-N(6)	122.9 (3)	122.7 (5)
C(8)-C(7)	1.395 (5)	1.378 (9)	C(4)-N(1)-C(3)	116.4 (3)	117.7 (5)
C(17)-C(16)	1.382 (5)	1.387 (9)	C(7)-N(5)-C(11)	117.8 (3)	118.5 (5)
C(16)-C(15)	1.390 (5)	1.387 (9)	C(13)-N(6)-C(17)	117.0 (3)	118.4 (5)
C(15)-C(14)	1.388 (5)	1.383 (9)	N(1)-C(3)-C(6)	123.0 (3)	123.3 (5)
C(14)-C(13)	1.386 (5)	1.384 (9)	N(5)-C(11)-C(10)	121.7 (3)	120.7 (5)
			N(6)-C(17)-C(16)	122.8 (3)	121.7 (5)
			N(1)-C(3)-C(5)	115.2 (3)	116.0 (5)
			N(5)-C(11)-C(12)	114.7 (3)	116.7 (5)
			N(6)-C(17)-C(18)	115.3 (3)	117.0 (5)

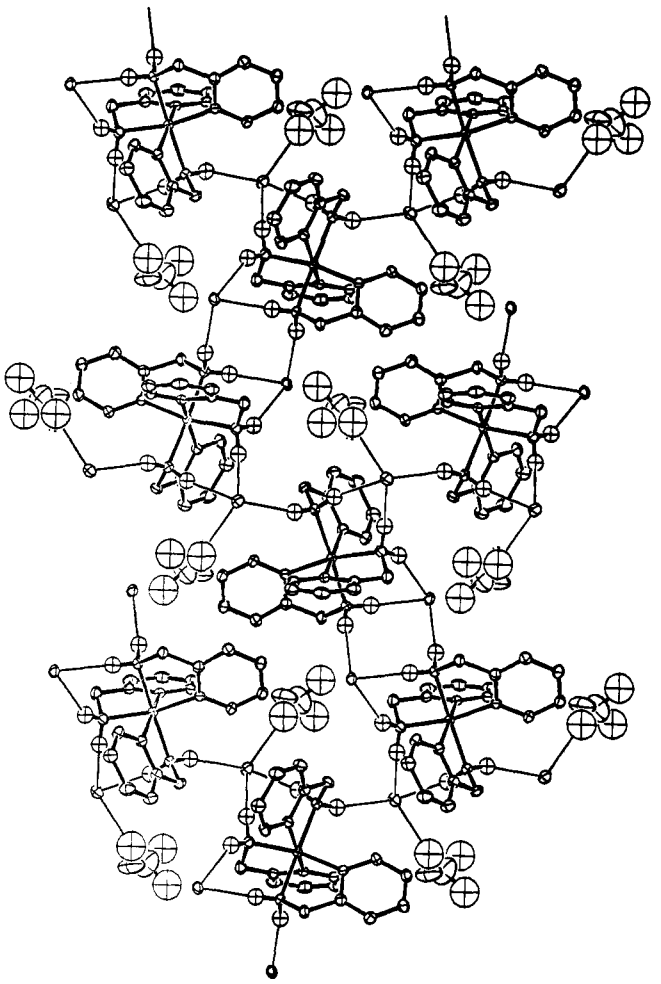

Figure 3. Packing diagram of $Fe(2\text{-pic})_3Cl_2 \cdot MeOH$ at 115 K showing two-dimensional hydrogen-bonding network. The projection is down the *b* axis with the *a* axis horizontal (from left to right) and the *c* axis vertical (from top to bottom).

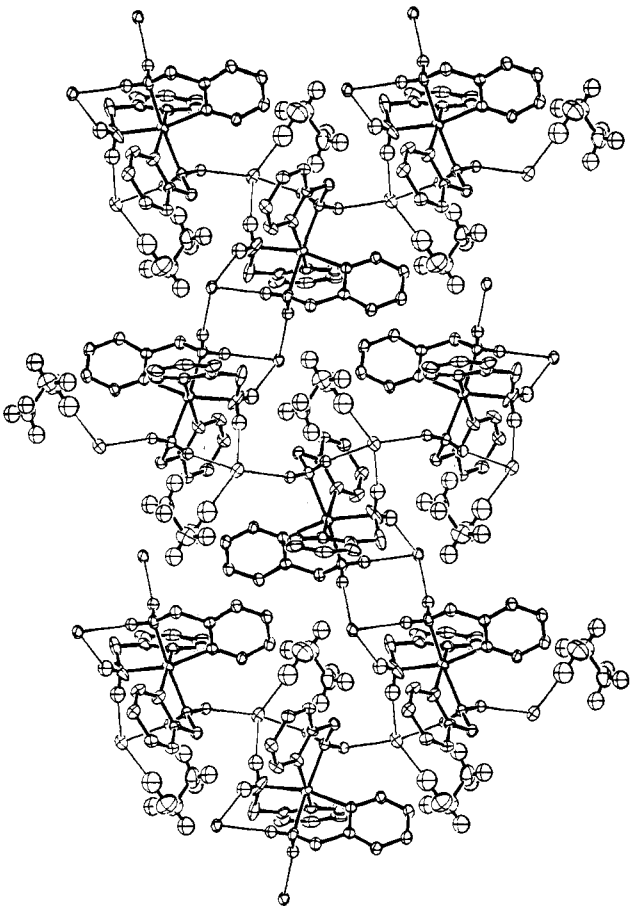

Figure 4. Projection perpendicular to the *ac* plane of $Fe(2\text{-pic})_3Cl_2 \cdot EtOH$ at 115 K showing the two-dimensional hydrogen-bonding network. The *a* axis is horizontal (from left to right) and the *c* axis vertical (from top to bottom).

Table VI. Iron-Nitrogen Bond Lengths (Å) in $Fe(2\text{-pic})_3Cl_2 \cdot EtOH$ at 115 K

amine	Fe-N(2)[a]	2.080 (4)
	Fe-N(3)	2.088 (4)
	Fe-N(4)[a]	2.010 (3)
	Fe-N(amine)	2.059 (4)
pyridine	Fe-N(1)	2.106 (4)
	Fe-N(5)[a]	2.080 (4)
	Fe-N(6)[a]	2.088 (4)
	Fe-N(pyridine)	2.091 (4)
	Fe-N(av)	2.075 (4)

[a] Trans.

mer isomer of this ion in tris(2-picolylamine)iron(II) diiodide. A more detailed comparison of these structures will be found in a companion paper.[16]

Another criterion by which the success of the spin isomer resolution can be judged is the limited correlation between the refined thermal parameters of corresponding atoms in the low-spin and high-spin ligands (see Table III). In the refinements of the 148 and 171 K structures, independent isotropic thermal parameters were assigned to all atoms in both high-spin and low-spin ligands. The fact that these parameters converge to chemically reasonable values, even in cases where the distances between high-spin and low-spin atoms are quite small, is rather remarkable.

The tris(2-picolylamine)iron(II) ion observed in the ethanol solvate has the same geometry as that observed in the methanol solvate (see Table VI). At 115 K, where there are significant amounts of both spin isomers, an average iron–nitrogen bond length of 2.075 (4) Å is observed.

Description and Comparison of the Hydrogen-Bonding Network in the Methanol and Ethanol Solvates

The same two-dimensional hydrogen-bonding network links the noncoordinating chloride ions to all six amine hydrogen atoms and to the alcohol molecules in the methanol and ethanol solvates. The remarkable similarity of the structures in a single sheet is demonstrated by comparison of Figures 3 and 4. The symmetry operations that relate components of a single sheet are the same in both structures; one chloride ion links complexes related by a glide plane and is hydrogen bonded to the alcohol, while the other joins complexes related by an inversion center. No hydrogen bonding occurs between adjacent layers. The structures differ in that in $Fe(2\text{-pic})_3Cl_2 \cdot MeOH$ the adjacent layers are related by 2_1 or glide operations (see Figure 5), whereas in $Fe(2\text{-pic})_3Cl_2 \cdot EtOH$ adjacent layers are related by a lattice translation. The NH-Cl bond lengths for the methanol solvate at the various temperatures are presented in Table VII and lie within the range previously observed.[22] The N-Cl distances range from 3.15 (1) to 3.45 (1) Å. The corresponding table for the ethanol solvate is included in the supplementary material.

Hydrogen-bond formation between the noncoordinating chlorides and the amine hydrogens in the tris(2-picolylamine)iron(II) dichloride solvates has been previously suggest-

Table VII. Hydrogen Bonding Interactions in $Fe(2\text{-pic})_3Cl_2 \cdot MeOH$

	115 K no groups	115 K groups	148 K	171 K	199 K	227 K
			Low Spin			
C11-N2H1[a]	2.29	2.28	2.31	2.32	2.30	2.30
C11-N2H2[b]	2.27	2.27	2.28	2.31	2.36	2.35
C11-N3H2[b]	2.42	2.42	2.49	2.50	2.47	2.45
C12-N3H1[c]	2.22	2.22	2.18	2.16	2.20	2.20
C12-N4H1[c]	2.42	2.42	2.38	2.31	2.38	2.11
C12-N4H2[d]	2.46	2.46	2.46	2.46	2.50	2.61
			High Spin			
C11-N2H1*[a]			2.26	2.27	2.30	2.29
C11-N2H2*[b]			2.27	2.27	2.28	2.28
C11-N3H2*[b]			2.31	2.34	2.38	2.37
C12-N3H1*[c]			2.33	2.29	2.27	2.28
C12-N4H1*[c]			2.51	2.47	2.43	2.47
C12-N4H2*[d]			2.40	2.39	2.41	2.38
			Methanol Molecule			
C12-OH	2.42					
C12-O	3.09	3.08	3.08	3.06	3.06	3.06

[a] $1/2 - x, -y, 1/2 + z$. [b] $1/2 + x, y, 1/2 - z$. [c] $1/2 - x, 1/2 + y, 1/2 - z$. [d] $1 - x, 1/2 + y, z$.

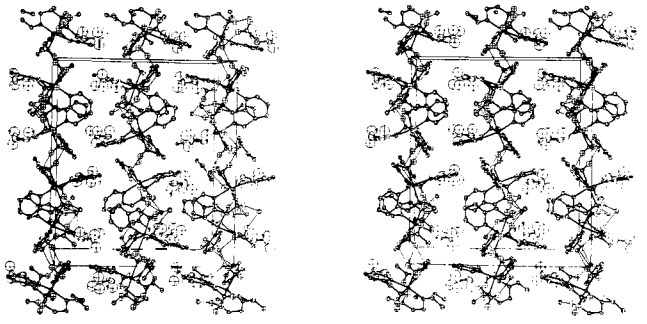

Figure 5. Stereoscopic ORTEP pair of the $Fe(2\text{-pic})_3Cl_2 \cdot MeOH$ lattice. The view is down the a axis with the b axis horizontal (from left to right) and the c axis vertical (from bottom to top).

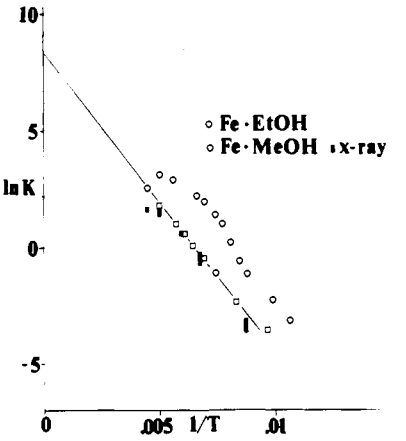

Figure 6. Equilibrium constant data for the low-spin to high-spin transformation of $Fe(2\text{-pic})_3Cl_2 \cdot MeOH$ obtained from Sorai et al. and from multiple temperature X-ray analysis of the methanol solvate. The equilibrium constants at 115, 148, 171, and 227 K were derived from data collected as the crystal was warmed from 115 K, whereas that at 199 K was obtained when the crystal was cooled from room temperature.

ed.[14,23] The nature of the hydrogen-bonding network in the crystal lattice of a spin transition compound can markedly influence the spin equilibrium behavior. The crystallographic[7] and solution studies[24] of iron(III) spin transition complexes indicate that solvent-HN-Fe(III) hydrogen bonding interactions favor the low-spin state, where solvents producing the strong [S···HN] hydrogen-bonding interactions also produced the greatest low-spin isomer populations.

Thermodynamic Behavior

Although there appear to be some systematic differences between the spin transition equilibrium constants obtained crystallographically for $Fe(pic)_3Cl_2 \cdot MeOH$ and those estimated from Mossbauer measurements[23,25] (see Figure 6), both studies indicate that the transition in the methanol solvate is essentially noncooperative. Our least-squares fit of the Mossbauer measurements published by Sorai et al. yields ΔH and ΔS of 2.35 (8) kcal/mol and 15.3 (8) eu, respectively. These thermodynamic values can be compared with ΔH and ΔS of 4 kcal and 10 eu for the spin transition in the tris(4-(6-R)-2,2-pyridyl)-3-azabutenylamine iron(II) complex[9] in the solid state and in solution, with values of 3.8 kcal and 11.4 eu in a tridentate complex of hydrotris(1-pyrazolyl)borate with Fe(II)[26] in solution, and with 3.91 kcal and 14.8 eu for aqueous bis(2,2-pyridylamino)-4-(2-pyridylthiazole)iron(II) chloride.[27] Enthalpy changes close to 4 kcal/mol in the three examples cited probably reflect the fact that all these materials undergo spin transitions near room temperature. In general the enthalpy change associated with a spin transition in the solid state is very sensitive to specific intermolecular interactions. On the other hand, it is reasonable to expect that the entropy change will not be strongly lattice dependent.[28]

Cooperativity

Unlike the methanol solvate, the ethanol solvate undergoes a cooperative spin transition, as seen in the sigmoidal dependence[23] of $\ln K$ on $1/T$ (Figure 6) derived from Mössbauer measurements by Sorai et al.[30] Mikami et al. have very recently determined the structure of the ethanol solvate at 298, 150, and 90 K and observed an order-disorder transition in the ethanol molecules.[32] They therefore account for the cooperative nature of the spin transition in the ethanol solvate in terms of a coupling of the spin transition with the order-disorder transition of the ethanol molecules.

Acknowledgment. This work was supported by the UCLA research committee, the UCLA Office of Academic Computing, and the National Science Foundation (CHE 78-01564). Bradley A. Katz was supported by a UCLA chancellor's fellowship, and Charles E. Strouse acknowledges the support of an Alfred P. Sloan research fellowship.

Supplementary Material Available: A listing of atomic positional and thermal parameters at each temperature for the methanol and ethanol solvates, bond distances and angles in the ethanol solvate, and a listing at each temperature of observed and calculated structure factors for the methanol and ethanol solvates (74 pages). Ordering information is given on any current masthead page.

References and Notes

(1) E. K. Barefield, D. H. Busch, and S. M. Nelson, *Q. Rev., Chem. Soc.*, **22**, 457 (1968).
(2) V. E. König, *Ber. Bunsenges. Phys. Chem.*, **76**, 975 (1972).
(3) L. Sacconi, *Pure Appl. Chem.*, **27**, 161 (1971).
(4) E. König, *Coord. Chem. Rev.*, **3**, 471 (1968).
(5) G. R. Hall and D. N. Hendrickson, *Inorg. Chem.*, **15**, 607 (1976).
(6) L. J. Wilson, D. Georges, and M. A. Hoselton, *Inorg. Chem.*, **14**, 2968 (1975).
(7) E. Sinn, G. Sim, E. V. Dose, M. F. Tweedle, and L. J. Wilson, *J. Am. Chem. Soc.*, **100**, 3375 (1978).
(8) E. König and K. J. Watson, *Chem. Phys. Lett.*, **6**, 457 (1970).
(9) M. A. Hoselton, L. J. Wilson, and R. S. Drago, *J. Am. Chem. Soc.*, **97**, 1722 (1975).
(10) J. G. Leipoldt and P. Coppens, *Inorg. Chem.*, **12**, 2269 (1973).
(11) L. M. Goldsmith and C. E. Strouse, *J. Am. Chem. Soc.*, **99**, 7580 (1977).
(12) J. P. Collman, T. N. Sorrell, K. O. Hodgson, A. K. Kulshrestha, and C. E. Strouse, *J. Am. Chem. Soc.*, **99**, 5180 (1977). This investigation revealed the presence of a mixture of high-spin and low-spin porphyrins in a material known to undergo a spin transformation. Further study has revealed, however, that these two species do not interconvert, but rather that one of them undergoes a spin transformation. Thus, the present investigation is the first report of the successful resolution of true spin isomers. A detailed account of the porphyrin investigation will be published in the near future.
(13) G. A. Renovitch and W. A. Baker, *J. Am. Chem. Soc.*, **89**, 6377 (1967).
(14) M. Sorai, J. Ensling, K. M. Hasselbach, and P. Gütlich, *Chem. Phys.*, **20**, 197 (1977).
(15) C. E. Strouse, *Rev. Sci. Instrum.*, **47**, 871 (1976).
(16) The structures of $Fe(2\text{-pic})_3Cl_2 \cdot 2H_2O$ and of $Fe(2\text{-pic})_3I_2$ will be published elsewhere.
(17) "International Tables for X-ray Crystallography", Vol. IV, Kynoch Press, Birmingham, England, 1974.
(18) J. Strouse, S. W. Layten, and C. E. Strouse, *J. Am. Chem. Soc.*, **99**, 562 (1977).
(19) The programs used in this work included data reduction programs written at UCLA; JBPATT, JBFOUR, and PEAKLIST, modified versions of Fourier programs written by J. Blount; UCLA versions of ORFLS (Busing, Martin, and Levy), structure factor calculations and full-matrix, least-squares refinement; ORTEP (Johnson), figure plotting; ABSN (Coppens), absorption correction; and ORFFE (Busing, Martin, and Levy), distance, angle, and error computations. The equations used in data reduction are the same as given in A. K. Wilkerson, J. B. Chodak, and C. E. Strouse, *J. Am. Chem. Soc.*, **97**, 3000-3004 (1975). All least-squares refinements computed the agreement factors R and R_w according to $R = \Sigma||F_o| - |F_c||/\Sigma|F_o|$ and $R_w = [\Sigma w_i||F_o| - |F_c||^2/\Sigma w_i|F_o|^2]^{1/2}$, where F_o and F_c are the observed and calculated structure factors, respectively, and $w_i^{1/2} = 1/\sigma(F_o)$. The parameter minimized in all least-squares refinements was $\Sigma w_i||F_o| - |F_c||^2$. All calculations were performed on the IBM 360-91KK computer operated by the UCLA Campus Computing Network.
(20) In each group, the methylene protons and the amine nitrogen and protons were allowed a linear distortion mode approximating a rotation. See C. Strouse, *Acta Crystallogr., Sect. A*, **26**, 604 (1970).
(21) An O-OH bond distance of 0.75 (8) Å and an OH-O-C bond angle of 101 (7)° were obtained at 115 K.
(22) K. Nakamoto, M. Margoslies, and R. E. Rundle, *J. Am. Chem. Soc.*, **77**, 6480 (1955).
(23) P. Gütlich, R. Link, and H. G. Steinhauser, *Inorg. Chem.*, **17**, 2509 (1978).
(24) M. F. Tweedle and L. J. Wilson, *J. Am. Chem. Soc.*, **98**, 4824 (1976).
(25) M. Sorai, J. Ensling, and P. Gütlich, *Chem. Phys.*, **18**, 199 (1976).
(26) J. P. Jesson, S. Trofimenko, and D. R. Eaton, *J. Am. Chem. Soc.*, **89**, 3158 (1967).
(27) J. K. Beattie, R. A. Binstead, and R. J. West, *J. Am. Chem. Soc.*, **100**, 3044 (1978).
(28) The hysteresis in the spin transition of $Fe(2\text{-pic})_3Cl_2 \cdot MeOH$ was manifested in the anomalous behavior of the lattice parameters with temperature. However, there was no significant difference between the low-spin occupancy factor at 227 K approached from the low-temperature limit (Is fraction = 0.164 (19)) and that at 199 K approached from room temperature (Is fraction = 0.183 (20)). Hysteresis in the spin transitions of $Fe(paptH)_2(NO_3)_2$[29] and of $Fe(2\text{-pic})_3Cl_2 \cdot H_2O$[14] has been recently observed, and various proposals for the source of this behavior have been put forward. Because of the difficulty encountered when cycling single crystals of the picolylamine complex through the transition, this aspect of the transition behavior has not been pursued in the present investigation. This observation, however, deserves further study.
(29) G. Ritter, E. König, W. Irler, and H. A. Goodwin, *Inorg. Chem.*, **17**, 224 (1978).
(30) Sorai et al., examining the cooperativity in $Fe(2\text{-pic})_3Cl_2 \cdot EtOH$, prepared a series of zinc-diluted lattices, $Fe\ Zn_{1-x}(2\text{-pic})_3Cl_2 \cdot EtOH$. With decreasing iron concentration, the plot of ln K vs. $1/T$ approached linearity. The high-spin limiting slope of ln K vs. $1/T$ for $Fe(2\text{-pic})_3Cl_2 \cdot EtOH$ is the same as that for the zinc-diluted lattice. This is reasonable in that a zinc lattice would be expected to resemble more closely a high-spin iron lattice than a low-spin one since Zn(II)-N bond distances are close to high-spin Fe-N bond distances. For example, in $Zn(py_3\text{-tach})^{2+}$ and in $Zn(py_3TPN)^{2+}$, the Zn-Npy bond distances are 2.25 and 2.16 Å, respectively, while the Zn-aldimino nitrogen bond lengths are 2.15 Å in both complexes.[31]
(31) E. B. Fleischer et al., *Inorg. Chem.*, **11**, 2775 (1972).
(32) M. Mikami, M. Konno, and Y. Saito, Abstracts, National Meeting of the American Chemical Society, Honolulu, Hawaii, April 1979.
(33) During preparation of this manuscript a room temperature X-ray diffraction study of the dihydrate and methanol solvates of $Fe(2\text{-pic})_3Cl_2$ appeared: A. M. Greenaway and E. Sinn, *J. Am. Chem. Soc.*, **100**, 8080 (1978). The space group reported in this paper for the methanol solvate contains a typographical error.

Formation of Hydridocyclotriphosphazenes via the Reactions of Organocopper Reagents with Halocyclotriphosphazenes. Reaction Mechanism[1-3]

Harry R. Allcock* and Paul J. Harris

Contribution from the Department of Chemistry, The Pennsylvania State University, University Park, Pennsylvania 16802. *Received April 30, 1979*

Abstract: 1-Hydrido-1-alkyltetrachlorocyclotriphosphazenes, $N_3P_3Cl_4RH$ (11) (where R = CH_3, C_2H_5, *n*-C_3H_7, *i*-C_3H_7, *n*-C_4H_9, *i*-C_4H_9, *t*-C_4H_9), have been synthesized by the new reaction of hexachlorocyclotriphosphazene, $(NPCl_2)_3$, with alkyl Grignard reagents in the presence of $[(n\text{-}C_4H_9)_3PCuI]_4$, followed by treatment with 2-propanol. The structural characterization of these compounds is discussed together with a detailed study of the reaction mechanism that permits hydridophosphazene formation. These reactions proceed via the formation of metallophosphazene intermediates. The nature of these complexes is discussed.

An important need exists for the development of new synthetic methods for the preparation of cyclic or open-chain phosphazenes that contain alkyl or aryl groups bonded directly to the skeleton through phosphorus-carbon bonds. Cyclic alkyl- or arylphosphazenes are of interest for fundamental reactivity studies, as models for thermally stable high polymers, or as "monomers" for polymerization studies.[4] The high polymers themselves are expected to constitute a new class of useful macromolecules.

A number of examples have been reported in the literature of reactions between halophosphazenes and Grignard or organolithium reagents.[5-18] Such reactions lead to alkylation or

0002-7863/79/1501-6221$01.00/0